Remote Sensing of Land Degradation: Experiences from Latin America and the Caribbean

G. Metternicht* United Nations Environment Programme
J. A. Zinck International Institute for Geo-Information Science and Earth Observation
P. D. Blanco and H. F. del Valle Centro Nacional Patagónico

Land degradation caused by deforestation, overgrazing, and inappropriate irrigation practices affects about 16% of Latin America and the Caribbean (LAC). This paper addresses issues related to the application of remote sensing technologies for the identification and mapping of land degradation features, with special attention to the LAC region. The contribution of remote sensing to mapping land degradation is analyzed from the compilation of a large set of research papers published between the 1980s and 2009, dealing with water and wind erosion, salinization, and changes of vegetation cover. The analysis undertaken found that Landsat series (MSS, TM, ETM+) are the most commonly used data source (49% of the papers report their use), followed by aerial photographs (39%), and microwave sensing (ERS, JERS-1, Radarsat) (27%). About 43% of the works analyzed use multi-scale, multi-sensor, multi-spectral approaches for mapping degraded areas, with a combination of visual interpretation and advanced image processing techniques. The use of more expensive hyperspectral and/or very high spatial resolution sensors like AVIRIS, Hyperion, SPOT-5, and IKONOS tends to be limited to small surface areas. The key issue of indicators that can directly or indirectly help recognize land degradation features in the visible, infrared, and microwave regions of the electromagnetic spectrum are discussed. Factors considered when selecting indicators for establishing land degradation baselines include, among others, the mapping scale, the spectral characteristics of the sensors, and the time of image acquisition. The validation methods used to assess the accuracy of maps produced with satellite data are discussed as well.

Land Degradation Defined

Land degradation is a long-term loss of ecosystem function and services, caused by disturbances from which the system cannot recover unaided (UNEP, 2007). Direct effects include losses of soil organic carbon, nutrients, soil water storage and regulation, and belowground biodiversity. Indirectly, it means a loss of the land's productive capacity and wildlife habitat. Soil deterioration is one critical aspect of land degradation, particularly of irreversible land degradation leading to desertification. Soil degradation is a consequence of depletive human activities and their interaction with natural environments, resulting in soil quality decline. Lal and Stewart (1990) distinguish three types of soil degradation, namely physical (e.g., soil erosion by wind and water), chemical (e.g., salinization, acidification), and biological (e.g., decline in soil organic matter). Although there is consensus that soil degradation is often a severe issue, there are few systematic measurements of its extent and severity (UNEP, 2007).

Land degradation caused by deforestation, overgrazing, and inappropriate irrigation practices affects about 16% of LAC (UNEP, 2007). The problem is more severe in Meso-America where it affects 26% of the territory, while 14% of South America is affected (UNEP, 2004). About 22% of the arid regions of South America are affected by severe or very severe desertification resulting from the combination of soil and climate constraints, excessive grazing, bush clearing, forest and grassland fires, firewood gathering, and other extractive activities (Dregne, 1986). Water erosion is the main cause of land degradation, while wind erosion is significant in some locations such as the area bordering Bolivia, Chile, and Argentina (WRI, 1995). Salinization of agricultural soils due to irrigation is particularly significant in Argentina, Cuba, Mexico, and Peru, which have extensive dryland areas that are often sub-

Published in J. Environ. Qual. 39:42–61 (2010).
doi:10.2134/jeq2009.0127
Published online 1 Dec. 2009.
Received 6 Apr. 2009.
*Corresponding author (graciela.metternicht@unep.org).

677 S. Segoe Rd., Madison, WI 53711 USA

G. Metternicht, United Nations Environment Programme, Regional Office for Latin America and the Caribbean, Clayton, City of Knowledge- Avenida Morse, Edificio 103, Panamá City, Panamá. J.A. Zinck, International Institute for Geo-Information Science and Earth Observation (ITC), Enschede, Netherlands. P.D. Blanco and H.F. del Valle, Centro Nacional Patagónico (CENPAT), Consejo Nacional de Investigaciones Científicas y Técnicas (CONICET), Área Científica Ecología Terrestre; Boulevard Almirante Brown 2915, (U9120ACF) Puerto Madryn (Chubut), Argentina.

Abbreviations: FI, frequency index; GLADA, Global Assessment of Land Degradation and Improvement; GLASOD, Global Assessment of Human-induced Soil Degradation; NDVI, Normalized Difference Water Index; NDWI, Normalized Difference Water Index; NPP, net primary production; PI, polarization index; SRTM, shuttle radar topographic mission; VSW, vegetation soil and water.

jected to inappropriate use or protracted droughts (UNEP, 2004). Furthermore, the Global Environmental Outlook produced by UNEP (2007) identifies agricultural intensification to satisfy increasing demands in food, raw materials, and bioenergy as a cause of soil nutrient depletion.

Assessment Techniques

Common methods for assessing land degradation as identified in the LADA-FAO approach (Koohafkan et al., 2003) include: expert judgment, remote sensing, productivity changes, field monitoring, pilot studies at farm level based on field criteria and expert opinion, and modeling. Table 1 shows the relationship between methods and survey scales. In practice, synergistic uses combining several of these approaches are more common than the implementation of individual methods.

Early land degradation assessments were essentially based on expert judgment, as in the case of the Global Assessment of Human-induced Soil Degradation (GLASOD). In spite of the assessment drawbacks highlighted by Sonneveld and Dent (2009), the GLASOD approach is still used for estimating land degradation at global, regional, and national scales. However, over the last two decades, scientists and international agencies such as FAO, UNEP, and GEF have joined efforts to develop standardized, operational methods and tools to map and monitor land degradation at different scales. Significant advances occurred especially in the last decade with the wide application of geospatial technologies to study the causes, impacts, and trends of land degradation. Good examples of such applications are the FAO-WOCAT (World Overview on Conservation Approaches and Technologies) (FAO, 2003) and the GLADA (Global Assessment of Land Degradation and Improvement) (Bai et al., 2008a) approaches.

The benefit of remotely sensed data in the form of aerial photographs and satellite imagery has been well recognized for (i) assessing the spatial and temporal distribution of land degradation features and (ii) collecting input data for process simulation models to produce land cover maps, vegetation cover maps, bare soil fraction maps, and net primary production maps, among others. Land degradation results in adverse effects of which the spatial and temporal variations must be assessed. Knowledge of the processes of land degradation, process-controlling variables, and effects of degradation is a prerequisite to determine what information can be derived from remotely sensed images.

The processes leading to land degradation can be detected and assessed through indicators, which are measurable characteristics providing information about a condition, change of quality, or change in state of something valued (Dumanski and Pieri, 1996). The main challenge is to select indicators that are sufficiently representative and, at the same time, easy to understand and measure on a routine basis (Ponce Hernandez, 2002). Furthermore, the indicators should be SMART, that is, specific, measurable, achievable, and time-bound (Schomaker, 1997). Indicators can be collected using a variety of techniques, including geo-referenced field observations (GPS), laboratory determinations, remotely sensed data, or a combination thereof.

Surveys assessing the current status of the land in terms of ongoing degradation processes aim at determining the spatial variability and condition of the natural vegetation (coverage, structure), agricultural crops (performance, coverage), soil surface (sealing, crusting), and soil erosion surface features (gully, rill, and sheet erosion). Monitoring changes over time involves characterizing surface dynamics such as the development of crop canopy over a growing season as an indirect indicator of erosion, or the long-term formation of rills and gullies in an area. Likewise, process-controlling variables such as rainfall interception, canopy water storage, and changing agricultural land use through seasons can be derived from air- or satellite-borne images that can be used as information in process simulation models of land degradation.

This paper reviews a large set of publications that report on remote sensing research undertaken in Latin America and the Caribbean since the early 1980s for mapping land degradation caused by water (including debris flows and landslides) and wind erosion, salinization, and disturbance of the vegetation cover. Emphasis is put on the selection and remote identification of indicators for mapping and monitoring land degradation features and processes. We first provide a summary on sensors and mapping scales used for assessing land degradation. Then we analyze experiences of mapping land degradation caused by soil erosion, salinization, and alteration of the vegetation cover, and we highlight the approaches used for data capture, transformation, and display.

Sensors, Mapping Scales, and Extent of Mapped Areas

A variety of remote sensors have become available to the scientific community during the past 30 yr, with the potential to provide useful information for assessing land degradation. Such sensors are usually classified according to the source of energy (passive or active sensors), the type of platform (ground-, air-, or space-borne), the region of the spectrum used to image the earth's surface (optical, infrared, microwave), the platform trajectory (sun-synchronic or geo-stationary satellites), the number and width of spectral bands (panchromatic, multispectral, hyperspectral), the spatial resolution (high, medium also known as Landsat-like, low), the spatial coverage (point or image view), the temporal resolution (hourly, daily, weekly revisiting frequency), and the radiometric resolution (8, 12, 16, 32 bits) (Metternicht, 2007).

This work compiled and analyzed over 60 research papers to determine remote sensors usage vs. land degradation type and scale of the studies undertaken in Latin America and the Caribbean. Tables 2, 3, 4, and 5 synthesize this effort, showing that the Landsat series (MSS, TM, ETM+) is nowadays the most commonly used data source (49%), followed by aerial photographs (39%), and microwave sensing (ERS, JERS-1, Radarsat) (27%). About 43% of the works analyzed use multi-scale, multi-sensor, multi-spectral approaches to the cartography of degraded areas, with a combination of visual interpretation and advanced image processing techniques. The use of more expensive hyperspectral and/or very high spatial resolution

Table 1. Common methods for assessing land degradation.

Method	Scale	Comments	Application examples
Expert judgment	Global, small scale	· Subjective, particularly in the definition of degradation classes: not degraded; slight, moderate, severe, very severe degradation · Hardly reproducible · Relatively low cost	Global: GLASOD† Regional: A co-evolutionary approach is used to explain the fate of African soils, focusing especially on the interaction between short-term local and long-term global processes (Koning and Smaling, 2005). National: The mapping approach is based on the time series analysis of satellite data. Vegetation dynamics is characterized using NDVI estimates from the coarse scale, hyper-temporal 1-km MEDOKADS archive, which is based on calibrated NOAA–AVHRR images (Hill et al., 2008). National: Use of expert judgments to conduct a water erosion hazard assessment in Ethiopia (Sonneveld, 2003). Local: Evaluation of the soil erosion process using expert decision trees and artificial neural networks in traditional crops, Andalucia, southern Spain (De La Rosa et al., 1999).
Remote sensing	Global, regional, subregional and local	· Acquisition on a repetitive basis enables monitoring · Clear identification of indicators (direct or indirect) is needed · Indicator must carry direct spectral absorption features or be correlated to a soil chromophera · Cost varies with platform and sensor used	Global: GLADA Regional: Application of remote sensing to soil surface characterization by different wavelengths, temporal changes of surface states, incision and geometry of possible water pathways on the surface in Normandy (France) (King et al., 2005). Subregional: Mapping of wind erosion-related features in Patagonia (Argentina) (Blanco et al., 2009). Local: Hyperspectral data are used to derive soil chemical properties, organic matter, mineralogical content, infiltration capacity, aggregation capacity, and runoff coefficient in a catchment area, Brandenburg region (north-eastern Germany) (Chabrillat et al., 2003).
Field monitoring	Subnational, large scale	· Costly, depending on the intensity of fieldwork · Stratified sampling recommended · Enables monitoring over time	National: Evaluation of the Local NPP Scaling (LNS) method, where the NDVI sum (ΣNDVI) of the growing season, a surrogate for productivity, of each pixel was expressed relative to the highest values (90th percentile) of ΣNDVI observed in all pixels falling within the same land capability unit (LCU) (Wessels et al., 2007). Subnational: Comparison of historical and current soil salinity maps, using historical field and laboratory data in the Gorgan Region, Northeast Iran (Naseri, 1998). Local: Soil loss and runoff were assessed in five land units (LUs) of a closed basin by means of 18 experimental plots within a 42-mo period (Rostagno et al., 1999).
Productivity changes	National, local	· Uses crop performance indicators, biomass production related to land degradation as an expression of lowered productivity · Productivity decline could be caused by factors other than land degradation · Reliable data sources are required (e.g., national yield statistics, yield monitoring, etc.)	National: Potential areas of severe land degradation are identified with net primary productivity and rain-use efficiency in Kenya (Bai and Dent, 2006). Local: Reduction in crop yield, New Mexico (Madrigal et al., 2003; Lobell et al., 2007).
Pilot studies at farm level	Local	· Enables a grass roots view on the severity of degradation and its causes · Relying on field indicators of degradation can be subjective · Can be costly depending on area coverage	Dendrogeomorphological analysis using exposed shrub roots to estimate soil erosion rates in rangelands (Chartier et al., 2009). Quantification of visual soil erosion indicators (splash pedestals, sheetwash, rills, sedimentation, red color and stoniness) to evaluate soil loss in the Gikuuri catchment, Kenya (Okoba and Sterk, 2006).
Modeling	Global to local	· Uses established models for soil erosion by wind and water · Enables the integration of biophysical with socio-economic factors · Prediction of degradation hazard	IMAGE: land degradation model developed for describing current and future global water erosion. Sensitivity to water erosion computed from terrain erodibility, rainfall erosivity and land cover (Hootsmans et al., 2001). PESERA, WATEM-SEDEM, SPADS: comparison of these three spatially-distributed models for the prediction of soil erosion and/or sediment yield at regional scales in Spain. (Vente et al., 2008). MIRSED: methodology for modeling regional and national patterns of hillslope-scale soil erosion rates in the UK using a minimum information requirement (MIR) version of Water Erosion Prediction Project (WEPP) (Brazier et al., 2001). FuDSEM: fuzzy-based dynamic soil erosion model to produce potential erosion maps at catchment scale (Cohen et al., 2008).

† GLASOD = Global Assessment of Human-induced Soil Degradation; NDVI, Normalized Difference Vegetation Index; GLADA, Global Assessment of Land Degradation and Improvement; NPP, net primary production.

sensors like AVIRIS, Hyperion (hyperspectral), SPOT-5, and IKONOS is limited to areas of 15 to 150 km^2.

Research of subregional extent (i.e., above 400,000 km^2), for outputs at scales between 1:250,000 to 1:1,000,000 and

Table 2. Wind erosion surveys using remote sensing.

Type of soil degradation	Indicators	Location	Survey area size	Sensors	Spatial scale	Acquisition year	Method/techniques	Accuracy assessment techniques	Authors
			km^2		m				
Wind erosion	Surface erosion features (lineal dunes, deflation areas, mounds associated to shrubs, desert pavement)	Patagonia Argentina	7,600	Aerial photographs.	1:40,000 1:150,000	1966	Photo and visual interpretation with field surveys.	Field surveys.	Winjnhoud and Monteith (1982)
Wind erosion	Wind streaks	Bolivian Altiplano	160,000	Aerial photographs. Landsat Shuttle Imaging Radar (SIR-A)	– 30 40	– – 1981	Visual analysis of SIR-A image. Geologic interpretation of Landsat images, aerial photographs, and topographic maps.	A field trip in 1983 provides the ground truth.	Greesley et al. (1989)
Wind erosion	Paleo-aeolian sand features	Brazilian Amazon	24,200	Landsat TM†	30	1986	Linear contrast stretching, Transformed Vegetation Index, Optimum Index Factor, PCA. Supervised maximum likelihood classification.	–	Carneiro Filho and Zinck, (1994)
Wind erosion	Sand dunes	San Luis Province, Argentina	2,610	Aerial photographs Landsat TM	1:50,000–1:20,000 30	1962 1992	Photo-interpretation and visual interpretation, patch analysis, and change detection by patches difference.	–	Collado (1999)
Wind erosion	Sand dunes	San Luis Province, Argentina	2,610	Landsat TM Landsat MSS	30 80	1992 1982	Geometric corrections, correction of striping, atmospheric correction, conversion of digital levels to reflectance values, Neural Network classification.	–	Collado (2000)
Wind erosion	Sand dunes	San Luis Province, Argentina	2,610	Landsat TM Landsat MSS	30 80	1992 1982	Geometric corrections, correction of striping, atmospheric correction, conversion of digital levels to reflectance values, Spectral Mixture Analysis.	–	Collado et al. (2000)
Wind erosion	Aeolian features	Puna Argentina	3,800	Landsat TM	30	–	Visual interpretation. Remote sensing data provides input into GIS for wind erosion risk assessment. Use expert knowledge to rank the risk factors.	–	Navone et al. (2000)
Wind erosion	Dunes	Northeastern Patagonia Argentina	1,231	Aerial photographs Landsat TM Landsat ETM+ AVIRIS	1:20,000–1:60,000 30 30 4	1969–1970 1986 2002 2001	Geometric corrections and co-registration. Supervised maximum likelihood classification. Temporal change detection by skeleton method for determining sand dune megapatch movement rate. Statistical analysis of wind patterns related to dune migration.	–	Del Valle et al. (2008)

† TM = thematic mapper.

Table 3. Water erosion surveys using remote sensing.

Type of soil degradation	Indicators	Location	Survey area size	Sensors	Spatial scale	Acquisition year	Method/techniques	Accuracy assessment techniques	Authors
			km^2		m				
Water erosion	Gullies	Mexican Volcanic Belt	492	Aerial photographs	1:25,000–1:50,000	1970–1983	Georeferencing, enhancements of image data. Supervised maximum likelihood classification of Landsat data integrated with TMU and slope data.	Error matrixes.	Bocco (1990)
				Landsat TM	30	1984			
Water erosion	Gullies	Transmexican volcanic belt	80	Aerial photographs	1:50,000	_	Photo interpretation and detailed field survey. Gully modelling	Field measurements	Vázquez-Selem and Zinck (1994)
Water erosion	Landslides	Coello valley Colombian Andes	1,250	Aerial photographs	1:50,000	_	Photo interpretation and detailed field survey. Landslide modelling	Laboratory and field data	Lopez and Zinck (1991)
Water erosion	Landslides	Colombian Cordillera	300	Aerial photographs	1:25,000–1:50,000	_	Geometric corrections and co-registration. Compare morfodinamic maps obtained from stereoscope pair of SPOT-Landsat and stereoscope pair or ERS-1 images.	Field work based upon aerial photographs.	Vargas Cuervo (1997)
				SPOT-XS	20	1989			
				Landsat TM	30	1988			
				SAR ERS-1	30	1992			
Water erosion	Debris flows, shallow soil slips, slumps	Puerto Rico	300	Aerial photographs	1:20,000	Multi-temporal	Photo interpretation integrated with field surveys, topographic and land use maps into GIS to evaluate frequency and distribution of landslides.	_	Larsen and Torres Sánchez (1998)
Water erosion	Flooding	Brazilian Amazon River	2,000,000	SMMR Nimbus-7 satellite (37GHz)	27,000	multi-temporal 1979–1987	Calculation of the difference between vertically and horizontally polarized brightness temperatures, estimation of flooded area at monthly intervals using a linear mixing model with three end-members (water, nonflooded land, and inundated floodplain).	River level estimations are compared by Pearson product-moment correlations.	Sippel et al. (1998)
Water erosion	Drainage density, water infiltration, declivity, ruptibility-plasticity	Taquari River Basin, Brazil	5,830	Landsat TM	30	_	Landsat visual interpretation integrated with geomorphology, topographic and geologic maps.	_	Veneziani et al. (1998)
Water erosion	Surface erosion features (pavements, gullies, rills, rock fragments, color, vegetation cover)	Sacaba Valley, Bolivia	100	Landsat TM	30	1994	SAR despeckle. Co-registration and resample to 15 m. Data fusion. Supervised maximum likelihood classification and signature separability evaluation.	Error matrixes with ground data.	Metternicht and Zinck (1998)
				JERS-1 SAR	18	1994			
Water erosion	Surface erosion features (pavements, gullies, rills, topsoil color, rock fragments, vegetation cover)	Sacaba Valley, Bolivia	100	Aerial photographs	1:25,000	_	Geometric corrections. Extraction of end-members by principal components method, integrated with visual interpretation of aerial photos and field surveys. Lineal spectral unmixing of Landsat data.	Analysis of the RMS error image.	Metternicht and Fermont (1998)
				Landsat TM	30	1994			
Water erosion	Flooding	Bolivian Amazon	250,000	Landsat TM	30	1997	Visual interpretation of TM color composite and radar color multitemporal composites.	_	Bourrel et al. (1999)
				Radarsat	50	1997, 1998			
				ERS 2	12,5	1996, 1997			
Water erosion	Erosion features (gully, rill, sheet erosion, badlands)	Trujillo, Venezuela	226	Aerial photographs	1:25,000. Output products: 1:50,000	_	Photo interpretation integrated with field surveys, geologic and vegetation maps.	Field surveys.	Diaz et al. (1999)

(cont'd)

Table 3. Continued.

Type of soil degradation	Indicators	Location	Survey area size	Sensors	Spatial scale	Acquisition year	Method/techniques	Accuracy assessment techniques	Authors
			km^2		m				
Water erosion	Flooding	Parana river, Argentina	375	Landsat TM to simulate SAC-C images.	180 (simulated SAC-C)	1994, 1998	Co-registration and calibration, visual interpretation of Normalized Difference Vegetation Index (NDVI) to discriminate susceptibility to flooding.	_	Giraut et al. (2000)
Water erosion	Flooding	Paraná Delta, Argentina	2,700	Radarsat/SAR	28,5	multi-temporal 1997-1998	Conversion digital number to backscatter coefficients, despeckle, co-registration and geometric correction, image segmentation. Comparison between supervised decision classifier and unsupervised ISODATA.	Error matrixes	Parmuchi et al. (2000)
				Landsat TM	28,5	1997			
Water erosion	Topsoil loss, accumulation zones	Central-Western Argentina	2,500	ERS-1	30	1998	Visual interpretation of Landsat. SAR Interferometry. Co-registration of outputs and visual interpretation of color composite image.	_	Maldonado et al. (2001)
				ERS-2	30	1998			
				Landsat TM	30	_			
Water erosion	Landslides scars, debris flows, natural dam and rock falls	Vargas State, Venezuela	40	Aerial photographs	3,513,888,889	1991	Photo interpretation. Geometric rectification, tone enhancements, and visual interpretation of IKONOS. Outputs are combined into GIS with planimetric data, contour lines, hydrology and vegetation types to evaluate the distribution of the scars.	_	De La Ville et al. (2002)
				IKONOS	4	1999			
Water erosion	Gullies	Maranhão State, Brazil	831	Aerial photographs	_	_	Photo-interpretation integrated with field surveys and laboratory analysis.	_	Guerra et al. (2002)
Water erosion	Landslides	Northern Argentina	15,000	Landsat TM	30	1986–2001	Co-registration, supervised maximum likelihood classification.	Confusion matrixes and Kappa index.	Paolini et al. (2002)
Water erosion	Flooding	Central Brazilian Amazon	17,000	JERS-1 SAR	12.5	multi-temporal 1995–1997	Resample to 100 m by wavelet decomposition, mosaic generation, co-registration, conversion digital number to radar backscatter, supervised classification.	_	Rosenqvist et al. (2002)
Water erosion	Laminar erosion features, gullies	São Paulo, Brazil	460	Aerial photographs	1:25,000	1962	Photo-interpretation, principal component analysis of Landsat image, DTM, topographical maps and field information are integrated in a GIS environment to produce the final cartography.	_	Carneiro and Souza (2003)
				Landsat TM	30	1992			
Water erosion	Flooding	Western Brazil, Eastern Bolivia and Northern Paraguay.	484,970	NOAA-AVHRR NDVI maximum value composites	8,000	_	Combined use of monthly precipitation and monthly maximum value composite NDVI to predict monthly river water level by stepwise multiple linear regression technique.	Data 1981-1994 for model construction and data 1994-2000 for validation.	Liu et al. (2003)

(cont'd)

Table 3. Continued.

Type of soil degradation	Indicators	Location	Survey area size	Sensors	Spatial scale	Acquisition year	Method/techniques	Accuracy assessment techniques	Authors
			km²		m				
Water erosion	Landslide scars	Santa Catarina, Brazil	105	Landsat TM SPOT HRV	30 20	_ _	Radiometric correction. Transformation from RGB to IHS, Principal Component analysis and Wavelet Transform fusion. Comparison between these techniques using visual interpretation, statistical analysis and automatic classification	_	Marcelino et al. (2003)
Water erosion	Shallow mass movements	La Trinidad, Nicaragua	25	Aerial photographs	1:25,000	_	Photo interpretation integrated with field surveys. The output shallow landslide map is integrated in a logistic regression model with geomorphology, slope and accumulated flow variables to generate susceptibility maps.	Field surveys.	Menendez Duarte et al. (2003)
Water erosion	Flooding	Pampean Region, Argentina	3,600	Terra-ASTER/VNIR DEM SRTM	15 30	_ _	Geometric and radiometric correction of Terra-ASTER. Generation of DEM 30 m from SRTM by interpolating and resampling, to estimate drainage pattern and inundation area, comparison with spectral indices from Terra-ASTER (NDVI, NDWI, VSW).	_	Azcurra et al. (2004)
Water erosion	Landslide scars	Southern Brazil	4	Aerial photographs	1:20,000	_	Photo interpretation to landslide and vegetation cover mapping. High resolution DEM (2 m) derived from aerial photos is used to generate topographic attributes. By comparing the output results a landslide potential index is defined. Implementation of SHALSTAB model using field experiments.	_	Fernandes et al. (2004)
Water erosion	Flooding	La Pampa Province, Argentina	30,000	Landsat TM SAC-C	30 175	_ multi-temporal 2001–2003	Geometric corrections, comparison between unsupervised ISODATA classifications of Landsat vs. SAC-C images.	Use photo-interpretation as ground truth.	Mieza et al. (2004)
Water erosion	Debris flows	Northwestern Nicaragua	20	Aerial photographs	1:40,000-1:60,000. Output results: 1:10,000	1996–1998	Photo interpretation integrated with field surveys. Data concerning regolith, landslides, slope and land use are integrated in a qualitative debris flow hazard assessment.	Field surveys.	Pallàs et al. (2004)

(cont'd)

smaller, tends to use satellite imagery provided by sensors of low spatial resolution such as MODIS, SAC-C, NOAA-AVHRR, SMMR Nimbus-7, and Wide Field Imager of the CBERS-2B. For instance, del Valle et al. (1998) mapped about 700,000 km² of degraded areas in the Argentinean Patagonia using NOAA-AVHRR-Large Area Coverage (LAC) data together with validation data from Landsat MSS.

Sensors of moderate spatial resolution, covering the optical and infrared regions of the electromagnetic spectrum, such as Landsat (TM, ETM+, MSS), SPOT (HVR, Xs, HRG), ASTER, and CBERS, have been applied to map areas of 30 to 250,000 km². The output scales of such studies range from local, catchment, country

Table 3. Continued.

Type of soil degradation	Indicators	Location	Survey area size	Sensors	Spatial scale	Acquisition year	Method/techniques	Accuracy assessment techniques	Authors
			km²		m				
Water erosion	Landslides	Southern Honduras	108	Aerial photographs	1:50,000	_	Registration. Photo and visual interpretation integrated with topographic maps to produce slope, aspect, land cover, and stream proximity maps. Outputs maps are combined following a hierarchical scheme to produce landslide hazard maps.	The model is validated in an adjacent watershed.	Perotto Baldiviezo et al. (2004)
				SPOT Pan	10	1998			
Water erosion	Landslides	São Pablo, Brazil	200	Landsat TM	30	1996	Geometric and atmospheric corrections, contrast enhancement, image ratio TM5/TM7, TM4/TM3 and TM4/TM1. Principal component transformation. Visual interpretation of output results integrated with field surveys.	Aerial photographs and field surveys.	Sestini and Florenzano (2004)
Water erosion	Gullies	Texcoco, Mexico	0.08	Color aerial photograph	1,5	1997	Photo-interpretation integrated with field surveys. Neural network classification, trained with the pixel values derived from RGB.	Confusion matrixes and Kappa index.	Trueba Espinosa et al. (2004)
Water erosion	Shallow landslides	Venezuelan Andes	110	Landsat TM	30	1992	Lineal spectral unmixing of Landsat data to produce land cover map. Output is integrated with topographic, precipitation and geologic data using Artificial Neural Networks to assessment the landslide risk potential.	Use a part of the data set to accuracy assessment.	Gómez and Kavzoglu (2005)
Water erosion	Landslides	Northwestern Nicaragua	473	Aerial photographs	1:40,000. Output results: 1:10,000	2000	Photo interpretation integrated with field surveys for generation of TMU and landslide inventory map. Outputs results are combined into GIS to development a landslide susceptibility map.	The model is validated in a test zone.	Guinau et al. (2005)
Water erosion	Landslides, debris flows and rock falls	Rio Mendoza Valley, Argentina	1,600	Aerial photographs	1:50,000, output map: 1:100,000.	1963	Photo and visual interpretation with field surveys to landslide zonification mapping. Output is integrated into a GIS with ranked lithology and slope angle maps to landslide susceptibility assessment.	Use landslides historical data.	Moreiras (2005)
				Landsat TM	30	1985, 1986, 1997, 2000			
Water erosion	Gullies, rills, sheet erosion	Brazilian Cerrados	100	ERS-1	30	1997	Calibration to obtain backscattering values, despeckle, co-registration. Interferometric decorrelation for detecting sheet and rill erosion, visual interpretation to locate gullies.	_	Vrieling and Rodrigues (2005)
				ERS-2	30	1997–1999			

(cont'd)

to regional levels (1:50,000–1:250,000). A study example at regional scale is the cartography of 250,000 km² of flooded areas in the Bolivian Amazon, using visual interpretation of Landsat and microwave data (Bourrel et al., 1999). Riedel et al. (2007) present

Table 3. Continued.

Type of soil degradation	Indicators	Location	Survey area size	Sensors	Spatial scale	Acquisition year	Method/techniques	Accuracy assessment techniques	Authors
			km^2		m				
Water erosion	Landslides	Sierra Norte de Puebla, Mexico	15	IKONOS	1	1999	Visual interpretation. NDVI generation and application of a fragmentation algorithm. Output results are integrated with a socio-economic vulnerability index, geologic and geomorphologic maps to produce a risk map.	Field data using a GPS.	Borja Baeza et al. (2006)
Water erosion	Flooding	Paraná Delta, Argentina	2,700	Envisat ASAR	30	2003–2004	Image calibration using BEST, co-registration and geometric correction, temporal filtered of backscattering images, vegetation-dependent flooding prediction based on the comparison between radiative transfer model simulations and ENVISAT backscattering of different flood conditions in two types of marshes.	Estimated water levels are compared with measured water levels.	Grings et al. (2006)
Water erosion	Landslides	Metropolitan Zone of Mexico City.	7,800	SRTM DEM	90, output map: 30 m.	_	Filling of voids and reconstruction of a DEM 30 m using TIN method, from SRTM. Morphometrics parameters are derived from the output and are integrated with soils, land use, precipitation data throughout a heuristic model in decision tree to define landslide susceptibility areas.	_	Lopez and Nuñez (2006)
Water erosion	Landslides, flooding	Baja California, Mexico	23,725	Landsat	30–60	Multitemporal 1973–1999	Radiometric correction and co-registration. Supervised classification and change detection analysis into GIS to define hazards areas for flooding and landslides.	_	Martínez Gutiérrez (2006)
				Terra-ASTER	15	2001			
Water erosion	Soil compaction, impeded drainage, sheet and rill erosion	Tucuman, NW Argentina	1,060	Air photos, Landsat, SPOT	Variable	1971–1991	Photo interpretation and detailed field survey	Laboratory and field data	Zinck (2006)
Water erosion	Gullies, rills, sheet erosion	Delta of the Paraná River	17,500	Landsat TM	30	1992–2002	Visual interpretation. Radiometric correction and co-registration. Supervised classification and change detection analysis into GIS. NDVI generation and application of a fragmentation algorithm.	Error matrixes and Kappa index	Kandus et al. (2006)
Water erosion	Flooding	Monte Alegre, Brazilian Amazon	14,400	CBERS-2/CCD	20	_	Geometric and radiometric correction, extraction of flood areas by application of mathematical morphologic operators to describe geometric structures.	_	Ishikawa and Silva (2007)

(cont'd)

Table 3. Continued.

Type of soil degradation	Indicators	Location	Survey area size	Sensors	Spatial scale	Acquisition year	Method/techniques	Accuracy assessment techniques	Authors
			km²		m				
Water erosion	Flooding	Western Brazilian Amazon	400	R99SAR	6	_	Geometric co-registration, mosaic generation, resample to 10 m, application of a speckle noise reduction algorithm, unsupervised semivariogram textural classification of different	Confusion matrixes are related to each multi-frequency (HH, HV and VV) L-band image mosaic.	Miranda et al. (2007)
Water erosion	Landslide traces	Sierra Norte de Puebla, Mexico	135	IKONOS	1	2000	Normalization of IKONOS images is followed by spectral indexes (NDVI, SBI) generation. Output results are integrated with DTM slopes in an algorithm to extract automatically landslide traces.	_	Ochoa Tejeda and Parrot (2007)
Water erosion	Landslide scars	São Pablo, Brazil	30	SPOT 5	20	_	Segmentation and classification based in Bhattacharya algorithm. Output results are associated to NDVI, followed by intersect operator regarding geologic and geomorphologic variables, to automatic recognition of landslide scars.	_	Riedel et al. (2007)
Water erosion	Landslides	Matagalpa, Nicaragua	700	Landsat TM	30	_	NDVI, land cover, and land use classes are derived from Landsat. Output results are integrated with slope and lithology maps, using a GIS-based fuzzy logic method to landslide susceptibility mapping.	_	Schernthanner (2007)
Water erosion	Gullies	Sacaba Valley, Bolivia	100	SPOT HRV	20	_	Spot imagery for generation of vegetation map. Application of Vazquez-Selem and Zinck model to map gully spatial distribution.	Error matrixes.	Sotomonte (2007)
Water erosion	Gullies	Brazilian Cerrados	100	Terra-ASTER	15–30	Two dates: March wet season, August dry season	Geometric and radiometric correction, comparison between maximum likelihood classifier (gullies and nongullies) applied to images of each season vs. a bitemporal classification.	Use a gully map obtained from a panchromatic QuickBird image and field data.	Vrieling et al. (2007)
Water erosion	Surface color (redness), coarse fragments	Coastal Cordillera of central Chile	800	SPOT-HRV	20	1998	Georeferencing, conversion of digital numbers to exo-atmospheric reflectance, radiometric corrections. Computation of Redness Index and Brightness Index. Statistical analysis to determine relations between indexes, field and ground radiometric data.	Error matrixes with ground data.	Mathieu et al. (2007)

(cont'd)

a local-scale application of moderate to high spatial resolution sensors (i.e., SPOT-5) for mapping water erosion indicators over an area of 30 km². Likewise, moderate spatial resolution microwave data from ERS, Radarsat, JERS, Envisat satellites, and orbital Shuttle SIR-A have been used for mapping degraded areas of 100 to 17,000 km² (see Tables 3 and 4, and Fig. 1).

Table 3. Continued.

Type of soil degradation	Indicators	Location	Survey area size	Sensors	Spatial scale	Acquisition year	Method/techniques	Accuracy assessment techniques	Authors
			km²		m				
Water erosion	Landslides	Guantánamo, Cuba	6,200	Aerial photographs	1:25,000	2000	Photo interpretation. Output result is integrated with causative factors (geomorphology, geology, soil, land use, relief, drainage density, road and fault distance, rainfall) using neural networks and spatial multi-criteria techniques to landslide susceptibility modeling.	Field surveys.	Castellanos Abella (2008)
				Landsat ETM+	30	2001			

† TMU = terrain mapping unit; DTM = digital terrain model; DEM, digital elevation model; SAR = synthetic-aperture radar; SAVI = Soil Adjusted Vegetation Index; NDVI= Normalized Difference Vegetation Index; NDWI= Normalized Difference Water Index; VSW = Vegetation-Soil-Water Index; SBI = Soil Brightness Index; TM= thematic mapper; TIN = triangulated irregular network; SRTM= Shuttle Radar Topography Mission.

Figure 1 shows the dominance of aerial photographs and very high spatial resolution sensors (2.5-m spatial resolution or better) to map land degradation over small areas, with a mode around 300 km^2. This concerns surveys at local scale, or as support for field verification in research performed at smaller scales (generally in areas larger than 10,000 km^2).

Water-Induced Erosion

Shallow mass movements, gullies, rills, sheet erosion, badlands, debris flows, soil slips, and slumps are the indicators most commonly used to assess soil degradation induced by water (Table 3). Visual interpretation of aerial photographs, either black and white (Movia, 1980; Díaz et al., 1999; Guerra et al., 2002) or color (Trueba Espinosa et al., 2004), continues being a popular technique regardless of the size of the surveyed area (1–160,000 km^2). Time series of images taken by a video-camera attached to a balloon at 100-m elevation have also been used to monitor changes taking place at gully heads, and to estimate the speed of gully head retreat (Palacio-Prieto and López-Blanco, 1994). Additionally, Table 3 shows several studies making use of multi-sensor approaches covering the optical-infrared regions of the spectrum (e.g., aerial photographs and Landsat TM) (Bocco, 1990; Metternicht and Fermont, 1998; Carneiro and Souza, 2003), though relatively few studies investigated the possibility of merging optical and microwave data to discriminate land degradation features. Works by Metternicht and Zinck (1998), investigating a synergistic use of JERS-1 and Landsat TM for mapping water-induced surface erosion features, and Navone et al. (2002) integrating Radarsat-1 and Landsat TM to assess land degradation are examples of the latter.

In regards to classification techniques, Table 3 shows supervised approaches incorporating maximum likelihood classifiers to be the most common (del Valle et al., 1998; Kandus et al., 2006; Vrieling et al., 2007), although alternative techniques have been increasingly used. For instance, Metternicht and Fermont (1998) applied linear spectral unmixing of surface erosion features such as pavements, rills, topsoil color, and rock fragments from a Landsat TM image; Trueba Espinosa et al. (2004) used backpropagation artificial neural networks to discriminate gullies from color aerial photographs; and Vrieling and Rodrigues (2005) used interferometric decorrelation of ERS-1/2 (C-band SAR data) for detecting sheet and rill erosion, while applying visual interpretation to map gullies. Frequently, image data are advantageously combined in a GIS with ancillary data (relevant properties of slope, terrain, rock, soil, and land use units) for mapping gully, rill, and sheet erosion, and predict their potential occurrence (Bocco, 1990; Vázquez-Selem and Zinck, 1994; Carneiro and Souza, 2003).

Historical time series of aerial photographs and satellite images, frequently at different scales, and thus needing harmonization, have been used for retrospective monitoring of land degradation. For instance, in a study performed in Tucuman province, northwest Argentina, fields put into farming at different periods of time were selected from an image series to detect subsequently, from field and laboratory data, trends in soil compaction, drainage impediment, and sheet erosion resulting from mechanized soya cultivation (Zinck, 2006; Recatalá-Boix and Zinck, 2008).

The mapping of flooded areas, a highly dynamic land degradation phenomenon, has been undertaken with a variety of sensors and image processing techniques. Usually, flood studies use multi-temporal imagery for seasonal, annual, or inter-annual monitoring of the flooding processes and mapping affected areas. Often, data from high temporal (daily) resolution and low spatial resolution sensors are combined. Table 3 indicates how Liu et al. (2003) combined NOAA-AVHRR NDVI maximum value composites with monthly rainfall data for predicting monthly water levels, while Sippel et al. (1998) processed data from the SMMR Nimbus-7 to map 2,000,000 km^2 of flooded areas, using the derivates of the imagery as input to a linear mixing model that could differentiate water bodies, flooded plains, and nonflooded areas. Other approaches summarized in Table 3 include merging multi-temporal optical, infrared, and microwave C-band data to map flooded areas using visual interpretation of enhanced imagery (Bourrel et al. (1999), and Parmuchi et al., 2000), and the use of image segmentation and ISODATA classifiers (Parmuchi et al., 2000). The spatial resolution of the sensors used in the latter studies was 30 m on average.

Multi-temporal microwave imagery of the JERS-1 (L-band) and Envisat ASAR (C-band) has been tested by Rosenqvist et al. (2002) and Grings et al. (2006), respectively, for mapping

Table 4. Multi-purpose soil degradation surveys using remote sensing.

Type of soil degradation	Indicators	Location	Survey area size	Sensors	Spatial scale	Acquisition year	Method/techniques	Accuracy assessment techniques	Authors
			km^2		m				
Wind/water erosion	Surface erosion features (lineal dunes, gullies, rills, sheet, landslides)	Patagonia Argentina	60,000	Aerial photographs.	1:40,000–1:100,000	_	Photo and visual interpretation with field surveys.	Field surveys.	Movia (1980)
				Landsat MSS	80	_			
Wind/water erosion	Soil erosion features, salinity/alcalinity	Mendoza Province, Argentina	150,000	Aerial photographs.	1:40,000–1:60,000	1982–1986	Photo and visual interpretation with field surveys.	–	Roig et al. (1991)
				Landsat MSS	80	1982–1986			
Wind/water erosion	Erosion features (gully, rill, sheet erosion, blowouts, pavements, degraded vegetation)	Catamarca Province, Argentina	1,100	Aerial photographs	1:35,000	_	NDVI†, PCA and IHS are derived from Landsat. Geo-referencing, despeckle and visual interpretation of radar image. Output results are integrated with field information and socio-economic factors into GIS to desertification assessment using knowledge-base driven models.	_	Navone et al. (2002)
				Radarsat-1	25	1997			
				Landsat TM	30	1993, 1997, 1998			
Wind/water erosion, Vegetation degradation	Wind, runoff, and vegetation spatial patterns	Northeastern Brazil	300	Aerial photographs	0.09–0.72	2002	Fourier signature (signal/noise ratio) of aerial photos to characterize the vegetation spatial arrangements. DEM 25 m derived from SAR interferometry, calculation of the potential runoff. Statistical analysis to determine relations between wind regime, runoff and vegetation patterns.	Field surveys.	Ares et al. (2003)
				ERS/SAR 1–2	30	_			
Wind/water erosion	Erosion features (blowouts, dunes, gullies, rills, sheet erosion, desert pavements)	Catamarca Province, Argentina	2,000	Radarsat/SAR	25	Wet and dry season	Calibration, enhancements and filters (Flee, Fmode, Fsharp y Fgamma) are applied in SAR images. Pre-processed images are visually and statistically compared with ground truth.	_	Navone and Palacín (2004)
Wind/water erosion	Wind streaks, dunes, gullies, erosion pavements	Northeastern Patagonia Argentina	1,231	ERS/SAR	25	1992–2002	Geometric and radiometric corrections, despeckle, visual interpretation.	_	Del Valle and Blanco (2006)
				SIR-C XSAR	25	1994			
				Radarsat-1	8	2005			
Vegetation degradation	Woody plant encroachment, nonphotosynthetic vegetation pattern, bare soil	Central Argentina	763	AVIRIS	4	_	Monte Carlo spectral mixture analysis of AVIRIS data to estimate bare soil, photosynthetic and nonphotosynthetic fractional covers.	Field measurements to correlate with the estimate data.	Asner et al. (2003)
Wind/water erosion, Vegetation degradation	Surface erosion features (blowouts, compaction, gullies, rills, rock fragments, vegetation cover)	Patagonia Argentina	780, 000	NOAA-AVHRR	1000	1986–1992	Radiometric and Geometric corrections, enhancements, rectification, mosaic generation. Unsupervised and supervised maximum likelihood classification.	Field work based on Landsat MSS image. Error matrixes	Del Valle et al. (1998)
Wind/water erosion, Vegetation degradation	Bare soil, sand dunes, shrub encroachment	Mendoza Province, Argentina	123	AVIRIS	4	_	AVIRIS atmospheric corrections, conversion to reflectance values. Co-registration with IKONOS image (1m). Linear spectral mixture analyses integrated with field surveys and ground radiometric measures.	_	Huete et al. (2002)

(cont'd)

flooded areas (2700–17,000 km^2), with prior co-registration of the imagery and conversion to backscattering values. Textural classification of multi-frequency L-band SAR imagery to identify flooded forests and other flooded vegetation types has

Table 4. Continued.

Type of soil degradation	Indicators	Location	Survey area size	Sensors	Spatial scale	Acquisition year	Method/techniques	Accuracy assessment techniques	Authors
			km²		m				
Wind/water erosion, Vegetation degradation	Bare soil, sand dunes, shrub encroachment	Mendoza Province, Argentina	123	EO-1 Hyperion	30	_	Hyperion destriping, atmospheric corrections, conversion to surface reflectance. Co-registration with IKONOS image (1m). Spectral indexes calculation (NDVI, SAVI, First Derivative Vegetation Index). Linear spectral mixture analyses integrated with field surveys and ground radiometric measures.	_	Huete et al. (2003)
Wind/water erosion, vegetation degradation	Wind, runoff, and vegetation spatial patterns	Patagonia Austral	240,000	Landsat TM	30	1992–2002	Mixed classification: Supervised and unsupervised.	Field surveys. Error matrixes	Mazzoni and Vazquez (2004)
Wind erosion, vegetation degradation	Active and stabilized dunes, desert pavements, shrub encroachment	Northeastern Patagonia Argentina	300	Terra-ASTER Radarsat-1 Fine	15 8	2004 2005	Georeferencing, conversion to radiance values, PCA and SAVI calculations of optical data. Despeckle and extraction of textural measures from radar data. Data fusion. Multi-segmentation and object-oriented classification. Fuzzy comparison of output results.	Confusion matrixes and Kappa index.	Blanco et al. (2009)

† NDVI, Normalized Difference Vegetation Index; DEM, digital elevation model; SAR, synthetic-aperture radar; SAVI, Soil Adjusted Vegetation Index.

been another approach trialed by Miranda et al. (2007), while Grings et al. (2009) applied multitemporal analysis of AMSR-E signatures covering three ecosystems in the La Plata Basin to produce maps based on the normalized polarization index (PI) at C band and the normalized frequency index (FI) at C and Ka bands. Their study found wide regions characterized by higher PI values to be related to flooding along the Paraná River, while increased PI and FI values reflected the effect of a strong rainstorm in the Chaco forest.

Optical-IR imagery from moderate resolution sensors (e.g., Landsat TM, CBERS-2 CCD, Terra ASTER) have been used to identify flooded areas (3000–30,000 km²) using techniques as mathematical morphology (Ishikawa and Silva, 2007), unsupervised ISODATA classification (Mieza et al., 2004), and spectral indices like the NDVI, Normalized Difference Water Index (NDWI), and Vegetation Soil and Water (VSW) (Azcurra et al., 2004). The latter study also incorporated terrain information in the mapping process, by means of a DTM generated from Shuttle Radar Topographic Mission (SRTM) imagery with 30-m spatial resolution.

Landslide detection is the subject of a large number of research papers (15), as shown in Table 3. The mapping of landslides is primarily based on aerial photographs and optical-IR imagery from Landsat TM, ETM+, SPOT-5, and IKONOS satellites to cover areas ranging from 4 to 15,000 km². This type of imagery enables data outputs at scales of 1:10,000–1:100,000, which are often combined in a GIS with ancillary data (slope, aspect, land cover, land use, soils, geology, seismicity, proximity to streams) to produce landslide hazard maps (López and Zinck, 1991; de la Ville et al., 2002; Carvalho and Riedel, 2004; Perotto Baldiviezo et al., 2004; Guinau et al., 2005; Castellanos Abella, 2008; Castellanos Abella and Van Westen, 2008; Van Westen et al., 2008).

Photo-interpretation, geometric and radiometric corrections of satellite imagery, and contrast enhancement for visual interpretation are techniques commonly implemented, as evidenced in the works of Sestini and Florenzano (2004), who applied image transforms like Landsat TM band ratios and principal component analysis before visual interpretation of landslides; Marcelino et al. (2003) working with image transformations (e.g., RGB to IHS, principal components analysis and wavelet fusion) of Landsat TM data to discriminate landslide scars; and Ochoa Tejeda and Parrot (2007) using spectral indices from IKONOS imagery and a DTM for automated detection of landslide traces.

On the other hand, supervised maximum likelihood classifications have been applied to Landsat TM and Terra-ASTER imagery for mapping landslides (e.g., Paolini et al., 2002; Martínez Gutiérrez, 2006), whereas advanced classifiers like decision trees and neural networks were used by López and Nuñez (2006) and Castellanos Abella (2008), respectively, for landslide susceptibility modeling. Other studies to map landslide susceptibility have integrated thematic layers derived from Landsat TM imagery (NDVI, land cover and land use classes) with slope and lithology maps, using a GIS-based fuzzy logic classifier (Schernthanner, 2007), and image segmentation and classification of SPOT-5 imagery for mapping landslide scars (Riedel et al., 2007).

Spatial distribution analysis and hazard assessment of mass movements cannot be derived from remote sensing data alone. Image data must be combined with information on the en-

Table 5. Soil salinity surveys using remote sensing.

Type of soil degradation	Indicators	Location	Survey area size	Sensors	Spatial scale	Acquisition year	Method/techniques	Accuracy assessment techniques	Authors
			km^2		m				
Soil salinity-alkalinity	Proportion of chloride and sulfates present on the topsoil	Punata-Cliza Valley (Eastern Bolivian Andes)	90	Landsat TM	30	1996	Fuzzy set theory to define soil salinity classes; chloride, sulfate and carbonate anion ratios present in soil saturation extract are used to define classes. Georeferenced field samples are collected for laboratory determinations. Supervised maximum likelihood classification is applied to a Landsat TM†, whereby membership grades of saline fuzzy classes are incorporated as prior probabilities.	Error matrix, field samples collected for classification validation	Metternicht (2003)
Soil salinity	pH and EC; soil roughness	Punata-Cliza Valley (Eastern Bolivian Andes)	90	JERS-1 SAR L-band	12.5	1994	Fuzzy supervised classification; classes adopt transitional 'fuzzy' boundaries; field and laboratory determinations allow correlation of radar backscattering to soil surface roughness, the type and degree of soil surface salinity.	Error matrix and field survey	Metternicht (1998)
Soil salinity	Playa features Salt efflorescence and crusts Halophytic vegetation and salt-tolerant crops	Punata-Cliza Valley (Eastern Bolivian Andes)	90	Landsat TM	30	1996	Georeferenced field sampling and lab analyses. Determination of information classes based on EC, pH, and SAR data. Discrimination of salinity-alkalinity classes using transformed divergence analysis. Contextual analysis based on the relationship between landscape positions and salinity-alkalinity.	Error matrix and detection of spectral confusions	Metternicht and Zinck (1996, 1997)
Soil salinization	Salt efflorescence and crusts Halophytic vegetation	Former Lake Texcoco (Central Mexico)	60	Landsat ETM Air photos Ground-based spectroradiometer	30 2.6	2000 1999	EC maps using ordinary kriging, ground radiance measurements, and NDVI determinations. Data integration via a combined spectral response index (COSRI)	Field samples. Pearson correlation coefficient	Fernández Buces et al. (2009)
Soil salinity	Salinity and Sodicity classes	Chubut Valley, Argentina	413	SIR-C XSAR Radarsat-1	25 8	1994 2005	Radiometric and geometric corrections. Extraction of derived textural measures (mean euclidean distance, variance and skewness). Object-oriented image classification.	Field surveys. Error matrixes.	del Valle et al. (2009b)
Soil salinity	Salinity and sodicity classes	Chubut Valley, Argentina	64	ALOS AVNIR-2	10	2007	Geometric and atmospheric corrections, optical enhancement (Tasseled Cap). Radar-optical images fusión. Comparison between maximum likelihood classification vs. object-oriented classification.	Confusion matrixes and Kappa index.	del Valle et al. (2009a)

† TM, thematic mapper; SAR = sodium adsorption ratio; NDVI, Normalized Difference Vegetation Index.

vironmental factors that trigger and control landslides (e.g., rainfall, topography, soil properties, geologic setting, among others). In this sense, GIS plays a fundamental role as a platform to integrate multi-scale remote sensing, field survey, and ancillary data for detecting shallow landslides, debris flows, soil slips, and slumps, and for modeling landslide hazards (Tables 3 and 4). Geographic Information Systems (GIS) is also used in combination with artificial neural networks (Gómez and Kavzoglu, 2005), logistic regression (Menéndez-Duarte et al., 2003), and other advanced modeling techniques.

Wind Erosion

Sand dunes, wind streaks, paleo-aeolian features, desert pavements, sand encroachments, blowouts, and changes in the vegetation cover are indicators commonly applied for mapping wind-induced soil degradation. Land degradation is often assessed from a combination of wind and water erosion processes, a fact that may reflect the one-to-many relationship between indicators and processes, one indicator representing several processes, as highlighted by Metternicht (1996). Wind erosion is mapped alone in only 7 of the 14 works summarized in Table 2.

Traditionally, aerial photographs and Landsat imagery are combined to map wind erosion features over areas ranging from 1000 to 25,000 km^2, that is, at local and subregional levels (Winjnhoud and Monteith, 1982; Greesley et al., 1989). Visual interpretation of enhanced imagery (Navone et al., 2000), image transformation techniques (Carneiro Filho and Zinck, 1994), digital image classification using neural networks (Collado, 2000), spectral mixture analysis (Collado et al., 2000), and supervised maximum likelihood classification (Carneiro Filho and Zinck, 1994; del Valle et al., 2008) are some of the techniques applied for extracting data on wind erosion indicators. These data are subsequently used as input for GIS-based erosion risk assessment (Navone et al., 2000), temporal change detection of sand dune configuration (Collado, 1999), estimating sand mobilization rates, and statistical analysis of wind patterns related to dune migration (del Valle et al., 2008).

Multi-sensor (e.g., optical, infrared, and microwave), multi-scale approaches are applied for combined mapping of water- and wind-induced land degradation. For instance, Navone et al. (2002) combined various sorts of data such as field observations, aerial photographs, and Landsat/Radarsat satellite images to map erosion features; del Valle and Blanco (2006) identified wind erosion and deposition features (wind streaks, dunes, gullies, erosion pavements) using multi-temporal and multi-polarization microwave imagery of the ERS/SAR, Sir-C/X SAR, and Radarsat-1; and Blanco et al. (2009) applied image segmentation and object-oriented classifications of Terra-ASTER, and textural measures derived from Radarsat to discriminate desert pavements, active and stabilized dunes, and shrub encroachment.

Soil Salinization

Surface salinity is a highly dynamic property. This constrains the identification of salt-affected soils and the monitoring of the salinization process, because it influences the spectral, spatial, and temporal behavior of the salt features. Ground observations and radiometric measurements show that the main factors affecting the reflectance of salt-affected soils are quantity and mineralogy of salts, together with soil moisture, color, and surface roughness. Soil surface salinity can be detected from remotely sensed data, obtained by ground-based, airborne, or space-borne sensors, through direct indicators that refer to salt features visible at the soil surface and indirect indicators that refer to contextual features, such as the presence of native halophytic vegetation or the performance level of salt-tolerant crops (Metternicht and Zinck, 2003; Farifteh, 2007). Remote sensing-based approaches to map and monitor salinized landscapes should take into consideration (i) the discontinuous way in which salts tend to distribute on the landscape, so that appropriate classification schemes can be developed and (ii) the mineralogy of salt types, as this controls the occurrence of spectral absorption features in specific regions of the electromagnetic spectrum and influences the appearance of salinity indicators (e.g., salt crust types) at the soil surface (Metternicht and Zinck, 2009).

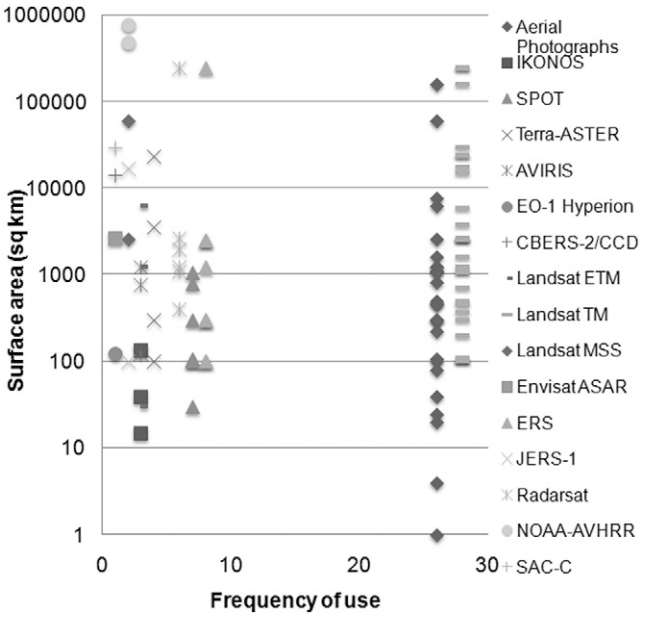

Fig. 1. Sensors used vs. surface areas covered by land degradation studies (Data source: Tables 2, 3, 4, and 5).

Metternicht and Zinck (2003, 2009) provide an extensive overview of the indicators and kinds of remotely sensed imagery commonly used for mapping soil and terrain salinization, whereas Ben Dor et al. (2009) review the use of airborne and satellite-borne sensors that have been used for mapping salt-affected areas.

In Latin America, the mapping of salt-affected areas began with the use of aerial photographs, and photo-interpretation is still a conventional technique for cartographies of medium to large scales. Fernández Buces et al. (2009) describe a synergistic approach that combines field and remote sensing data (Landsat ETM and color photographs) for mapping saline areas in Mexico, whereby a spectral response index using NDVI is used for image enhancement, before a combination with spectral responses of bare soil and vegetation (see Table 5).

Metternicht (1998) and del Valle et al. (2009b) provide examples of using microwave data for mapping soil salinization. Metternicht (1998) distinguishes saline from nonsaline surfaces in the Cochabamba Valley, Bolivia, using microtopographic terrain variations as an indirect indicator of salinity occurrence, when applying fuzzy classification to a set of JERS-1 data. Changes in soil surface roughness due to different salt crust types, the presence of halophytic vegetation, and soil aggregation due to cultivation practices facilitated the mapping process. Likewise, del Valle et al. (2009b) evaluated the use-

fulness of radar-derived parameters for detecting and mapping salt-affected soils under irrigation in Chubut (Argentina). Microwave imagery of the Radarsat-1 (C-band, HH polarization, acquired in 2005 with a spatial resolution of 8 m) and SIR-C (C- and L-bands, multi-polarization, acquired in 1994 with a pixel resolution of 25 m) were used to this end. Variables related to the radar system design (mainly wavelength, number of looks and polarization mode) and to the environmental setting of the area were analyzed to better understand the behavior of the radar backscattering. Four factors were significant when analyzing the variations of the backscattering coefficients in the environmental setting considered, namely soil type (soil texture), tillage conditions or soil surface aspect, soil moisture or surface water, and the presence of salts. The average backscattering values for all salt-affected soil classes were higher in the L-band than in the C-band of the SIR-C, when the same polarization modes were compared.

Vegetation Cover Degradation

Vegetation indices are a measure of greenness that has been successfully related to vegetation types and cover, biological changes of vegetation, leaf-area index, biomass, the fraction of photosynthetically active radiation absorbed by vegetation, crop production, net primary production, and vegetation changes, among others. In areas of closed vegetation canopy, the NDVI can be saturated. In sparsely vegetated areas typical of semiarid environments, retrieving quantitative information on vegetation type, cover, and biomass is more difficult because of the dominance of soil background reflectance and lack of the strong red edge that characterizes vegetation in humid regions (Paruelo et al., 2001; Okin and Roberts, 2004).

The Global Assessment of Land Degradation and Improvement (Bai et al., 2008b) proposes using the NDVI as a proxy of net primary production (NPP) for land degradation assessment at global and national levels. In South America, the approach has been tested in Argentina and Cuba (Bai and Dent, 2007a, 2007b). Changes in net primary production over 25 yr are computed using the GIMMS radiometer of the NOAA-AVHRR-Global Area Coverage (GAC) that has a spatial resolution of 8 km. Deviation from the norm is taken as an indicator of land degradation or improvement. The Global Inventory Modeling and Mapping Studies (GIMMS) data are combined with ancillary data indicative of rain use efficiency and energy use efficiency, and translated into NPP using MODIS NPP data at 1-km resolution. The MODIS NPP measures the fraction of the photosynthetically active radiation absorbed by the vegetation (Bai et al., 2008a). The authors highlight that long-term trends of NDVI derivates are unsophisticated indicators of land degradation, although the NDVI/NPP trend can provide a globally consistent baseline showing the places where significant biological change is happening (Bai et al., 2008b). Multi-scale, synergistic approaches are further needed to field-validate the results and determine the relationship between changes in NDVI/NPP and kinds of degradation. Furthermore, the coarse resolution of the GIMMS data is a limitation for accurate mapping, as an 8-km pixel is likely to integrate the signals from several landscape components. Many symptoms of severe degradation such as gullies and rills rarely cover large areas, thus degradation must be severe indeed to be seen against the signal of surrounding unaffected areas (Bai et al., 2008a).

Airborne hyperspectral imagery, with advanced image classification techniques (e.g., linear mixture modeling), has been used for mapping vegetation degradation and other indicators related to soil degradation over areas in the range of 100 to 1,200 km^2. Satellite hyperspectral Hyperion data have been processed using spectral indices (NDVI, SAVI, First Derivative Vegetation Index) and linear spectral mixture analysis integrated with field surveys and ground radiometric measures (Huete et al., 2003). Furthermore, Monte Carlo spectral mixture analysis of hyperspectral AVIRIS data has been applied to estimate photosynthetic and nonphotosynthetic fractional covers (Huete et al., 2002; Asner et al., 2003).

Validation

Assessing the accuracy of a particular method to map land degradation features and its prediction capability requires the validation of the resulting maps with independent data. Although the importance of accuracy assessment is widely recognized, this is, however, a difficult task mainly because of the significant investment in time and money needed to gather ground-truth information. It is thus not surprising that most of the reviewed studies have not or only slightly addressed the issue of validation (see Tables 2, 3,4, 5).

Tables 3 to 5 show that for those studies concerned with accuracy assessment of results, field data were the main source of ground-truth (e.g., Díaz et al., 1999; Menéndez-Duarte et al., 2003; Pallàs et al., 2004). Also, the interpretation of high resolution remote sensing imagery was used for validation, including aerial photographs (Mieza et al., 2004; Sestini and Florenzano, 2004) and high-resolution images such as panchromatic Quick-Bird (Vrieling et al., 2007).

The assessment of classification accuracy has generally been based on nonspatial statistics that are summarized in a confusion or error matrix, including overall accuracy, Kappa coefficient, variance, and Z statistics (Bocco, 1990; Metternicht and Zinck, 1998; Trueba Espinosa et al., 2004). However, none of these statistics explicitly considers the spatial distribution of misclassified pixels. Only a few studies provide information on the spatial distribution of classification errors (e.g., Metternicht and Fermont 1998; Blanco et al., 2009).

Conclusions

Early land degradation assessments were essentially based on expert judgment. Over the last decades, efforts have been made to develop standardized, operational methods and tools to map and monitor land degradation at different scales, with the wide application of geospatial technologies, in particular remote sensing. There is still a basic need to formalize degradation classes and select indicators that are unequivocally related to specific classes.

The problems faced in remote discrimination and mapping of surface features related to land degradation are: (i) the one-to-many relationships between surface features and land degradation processes, one feature being able to characterize several degradation processes; (ii) the spectral similarity among surface components associated with land degradation; and (iii) the differences in spatial resolution of the various data sources used for mapping purposes, including remotely sensed data, field observations, and laboratory determinations.

The constraints on remote sensing can be overcome by using indicators that directly or indirectly help recognize land degradation features in the optical, infrared, and microwave regions of the electromagnetic spectrum. Indicators must be selected taking into account the mapping scale, the spectral characteristics of the sensors, and the time of image acquisition. To support the performance of the selected indicators for pattern recognition, raw remotely sensed data are usually enhanced or transformed to improve the discrimination between degraded and nondegraded areas.

The contribution of remote sensing to mapping land degradation in LAC was summarized from the compilation of a large set of published research papers dealing with water erosion, wind erosion, salinization, and alteration of the vegetation cover (see Tables 3–5). The Landsat series (MSS, TM, ETM+) has shown as the most commonly used data source (49%), followed by aerial photographs (39%) and microwave sensing (ERS, JERS-1, Radarsat) (27%). About 43% of the works analyzed use multi-scale, multi-sensor, multi-spectral approaches to map degraded areas, with a combination of visual interpretation and advanced image processing techniques. The use of more expensive hyperspectral and/or very high spatial resolution sensors like AVIRIS, Hyperion, SPOT-5, and IKONOS tends to be limited to small areas.

Although Landsat-like digital data are nowadays common to land degradation studies, there is a rich experience in using analogical methods based on aerial photographs for identifying and mapping land degradation features. Some pioneering works, with their richness of details and accuracy of the observations, have not yet been beaten by automated or semi-automated techniques. Unfortunately, current scientific production tends to quote only the most recent papers, disregarding often earlier relevant works simply because of the time elapsed since their publication.

Shallow mass movements, gullies, rills, sheet erosion, badlands, debris flows, soil slips, and slumps are the indicators frequently used to assess soil degradation induced by water. Sand dunes, wind streaks, paleo-aeolian features, desert pavements, sand encroachments, blowouts, and changes in the vegetation cover are indicators commonly applied for mapping wind-induced soil degradation. Soil surface salinity is detected through direct indicators that refer to salt features visible at the soil surface, such as salt crusts and efflorescence, and indirect indicators that refer to contextual features, such as the presence of native halophytic vegetation or the performance level of salt-tolerant crops.

Visual interpretation of aerial photographs remains a popular technique for mapping land degradation features. Much progress has been made in the last decades thanks to synergistic multi-sensor approaches that combine visible, infrared, and microwave image data with ancillary data about environmental factors for mapping, modeling, and predicting land degradation. Likewise, a variety of transforms of remote sensing data has been used, including best band selection, principal components analysis, intensity-hue-saturation transformation, image ratioing, and image differencing. Band selection techniques such as the optimum index factor and transformed divergence analysis have been used for data preprocessing. Techniques used to recognize patterns or indicators related to land degradation range from visual interpretation of enhanced images to supervised and unsupervised approaches incorporating maximum likelihood classifiers, neural networks, decision trees, unmixing of surface features, fuzzy classification, and SAR interferometry techniques. Validation using ground-truth to assess the accuracy of remotely-sensed land degradation maps is still lagging behind. Detailed field surveys, although costly and time-consuming, are indispensable for this purpose. Alternative validation data provided by aerial photographs and high-resolution satellite imagery are increasingly used.

Acknowledgments

The authors are grateful to two anonymous reviewers, and David Lobell, whose thoughtful remarks and constructive comments have considerably improved this manuscript.

References

Ares, J., H.F. del Valle, and A.J. Bisigato. 2003. Detection of process related changes in plant patterns at extended spatial scales during early dryland desertification. Glob. Change Biol. 9:1643–1659.

Asner, G.P., C.E. Borghi, and R.A. Ojeda. 2003. Desertification in Central Argentina: Changes in ecosystem carbon and nitrogen from imaging spectroscopy. Ecol. Appl. 13:629–648.

Azcurra, D., P. Tchilinguirian, K. Hirose, T. Sanga, C.G. Asato, M. Kaku, and G.N. Candaosa. 2004. Análisis de inundación con datos ASTER y SRTM en la región de la laguna de La Picasa, Argentina. *In* Proc. Simposio Latinoamericano de Percepción Remota, 11th, Santiago, Chile. 22–26 Nov. 2004. SELPER, Bogotá, Colombia.

Bai, Z.G., and D.L. Dent. 2006. Global assessment of land degradation and improvement: Pilot study in Kenya. Rep. 2006/01. ISRIC-World Soil Information, Wageningen, the Netherlands.

Bai, Z.G., and D.L. Dent. 2007a. Land degradation and improvement in Argentina 1: Identification by remote sensing. Rep. 2007/05. ISRIC-World Soil Information, Wageningen, the Netherlands.

Bai, Z.G., and D.L. Dent. 2007b. Land degradation and improvement in Cuba. 1. Identification by remote sensing. Rep. 2007/04. ISRIC- World Soil Information, Wageningen, the Netherlands.

Bai, Z.G., D.L. Dent, L. Olsson, and M.E. Schaepman. 2008a. Global assessment of land degradation and improvement 1: Identification by remote sensing. Rep. 2008/1. FAO/ISRIC, Rome/Wageningen, the Netherlands.

Bai, Z.G., D.L. Dent, L. Olsson, and M.E. Schaepman. 2008b. Proxy global assessment of land degradation. Soil Use Manage. 24:223–234.

Ben Dor, E., G. Metternicht, N. Goldshleger, E. Mor, V. Mirlas, and U. Basson. 2009. Review of remote sensing-based methods to assess soil salinity. p. 39–60. *In* G. Metternicht and J.A. Zinck (ed.) Remote sensing of soil salinization: Impact on land management. CRC Press, Boca Raton, FL.

Blanco, P.D., G.I. Metternicht, and H.F. del Valle. 2009. Improving the discrimination of vegetation and landforms patterns in sandy rangelands: A synergistic approach. Int. J. Remote Sens. 30:2579–2605.

Bocco, G. 1990. Gully erosion analysis using remote sensing and geographic information systems. PhD diss. University of Amsterdam, Amsterdam, the Netherlands.

Borja Baeza, R.C., O. Esteban Chávez, J. Marcos López, R.J. Peña Garnica, and I. Alcántara Ayala. 2006. Slope instability on pyroclastic deposits: Landslide distribution and risk mapping in Zacapoaxtla, Sierra Norte De Puebla, Mexico. J. Mountain Sci. 3:1–19.

Bourrel, L., L. Philipps, and S. Moreau. 1999. Estudio de la dinámica de las inundaciones en la cuenca Amazónica Boliviana con un enfoque conjunto de la hidrología y de la percepción remota. *In* J-L Guyot (ed.) Hydrological and Geochemical Processes in Large Scale River Basins, Manaus, Brasil. 16–19 Nov. 1999. HIBam, en CDRom.

Brazier, R.E., J.S. Rowan, S.G. Anthony, and P.F. Quinn. 2001. MIRSED towards an MIR approach to modelling hillslope soil erosion at the national scale. Catena 42:59–79.

Carneiro, C.D.R., and J.J. Souza. 2003. Mapeamento geomorfológico em escala de semidetalhe da região de Jundiaí-Atibaia. Revista Brasileira de Geomorfol. 4:17–30.

Carneiro Filho, A., and J.A. Zinck. 1994. Mapping paleo-aeolian sand cover formations in the northern Amazon basin from TM images. ITC J. 3:270–282.

Carvalho, C.M., and P.S. Riedel. 2004. Análise da suscetibilidade a esgorregamentos nos entornos dos polidutos de Cubatão-SP, através de técnicas de informação geográfica. HOLOS Environ. 4:157–173.

Castellanos Abella, E.A. 2008. Multi-scale landslide risk assessment in Cuba. PhD diss. Utrecht University, Utrecht, the Netherlands.

Castellanos Abella, E.A., and C.J. Van Westen. 2008. Qualitative landslide susceptibility assessment by multicriteria analysis: A case study from San Antonio del Sur, Guantánamo, Cuba. Geomorphology 94:453–466.

Chabrillat, S., H. Kaufmann, B. Merz, J. Hill, and A.A. Mueller. 2003. Land degradation studies using spectroscopic techniques. Geophys. Res. Abstr. 5:12660.

Chartier, M.P., C.M. Rostagno, and F.A. Roig. 2009. Soil erosion rates in rangelands of northeastern Patagonia: A dendrogeomorphological analysis using exposed shrub roots. Geomorphology (in press).

Cohen, S., T. Svoray, J.B. Laronne, and Y. Alexandrov. 2008. Fuzzy-based dynamic soil erosion model (FuDSEM): Modelling approach and preliminary evaluation. J. Hydrol. 356:185–198.

Collado, A.D. 1999. Desertificación y dinámica espacio-temporal del paisaje dunar en la región central de San Luis, Argentina. p. 59–69. *In* Proc. Seminario Internacional sobre SIG y Teledetección Espacial aplicadas a la Ordenación del Territorio y el Medio Ambiente, Talca, Chile. 18–20 Nov. 1999. Departamento de Gestión Forestal y Ambiental, Universidad de Talca, Talca, Chile.

Collado, A.D. 2000. Spatio-temporal dynamics of dune patterns in semiarid Argentina: A neural network analysis. Edaphomatics Bull. no. 20. AICET-INTA, Buenos Aires, Argentina.

Collado, A.D., E. Chuvieco, and A. Camarasa. 2000. Satellite remote sensing analysis to monitor desertification processes in the crop-rangeland boundary of Argentina. J. Arid Environ. 52:121–133.

De La Rosa, D., F. Mayol, J.A. Moreno, T. Bonson, and S. Lozano. 1999. An expert system/neural network model (ImpelERO) for evaluating agricultural soil erosion in Andalucía region, southern Spain. Agric. Ecosyst. Environ. 73:211–226.

De La Ville, N., A. Chumaceiro Diaz, and D. Ramirez. 2002. Remote sensing and gis technologies as tools to support sustainable management of areas devastated by landslides. Environ. Dev. Sustain. 4:221–229.

del Valle, H.F., and P.D. Blanco. 2006. Indicadores espectrales del rango de las microondas para la evaluación y monitoreo de la erosión eólica. p. 65–84. *In* M. E. Abraham and G. Beekman (ed.) Indicadores de la desertificación para América del Sur. IICA-BID, Mendoza, Argentina.

del Valle, H.F., P.D. Blanco, and W. Sione. 2009a. Evaluación y monitoreo de la salinización de los suelos en la agricultura de regadío del noreste de Patagonia (Argentina). *In* D. Ponvert and D. Batista (ed.) La tecnología satelital de observación de la tierra en la evaluación, monitoreo y manejo de desastres naturales en la agricultura. Retos y perspectivas. INTA, Buenos Aires, Argentina.

del Valle, H.F., P.D. Blanco, W. Sione, C.M. Rostagno, and N. Elissalde. 2009b. Assessment of SALT-affected soils using multisensor radar data. A case study from Northeastern Patagonia (Argentina). p. 155–173. *In* G. Metternicht and J.A. Zinck (ed.) Remote sensing of soil salinization: Impact on land management. CRC Press, Boca Raton, FL.

del Valle, H.F., N.O. Elissalde, D.A. Gagliardini, and J. Milovich. 1998. Status of desertification in the Patagonian Region: Assessment and mapping from satellite imagery. Arid Soil Res. Rehabil. 12:95–122.

del Valle, H.F., C.M. Rostagno, F.R. Coronato, P.J. Bouza, and P.D. Blanco. 2008. Sand dune activity in north-eastern Patagonia. J. Arid Environ. 72:411–422.

Díaz, J., G. Royero, and G. Materano. 1999. Estado actual de erosión hídrica en la cuenca del río Motatán Sector Monay-Torococo–Mitón. Revista de la Facultad de Agronomía de la Universidad del Zulia, Maracaibo, Venezuela. 16:161–170.

Dregne, H.E. 1986. Desertification of arid lands. p. 4–34. *In* F. El-Baz and M.H.A. Hassan (ed.) Physics of desertification. Martinus Nijhoff Publ., Dordrecht, the Netherlands.

Dumanski, J., and C. Pieri. 1996. Application of the pressure-state-response framework for the land quality indicators (LQI) programme. *In* Land Quality Indicators and their Use in Sustainable Agriculture and Rural Development, Proc. of a Workshop, Rome. 25–26 Jan. 1996. Available at http://www.fao.org/docrep/w4745e/w4745e08.htm (verified 24 Nov. 2009). FAO, Rome.

FAO. 2003. Data sets, indicators and methods to assess land degradation in drylands. Rep. of the LADA e-mail Conf. FAO, Rome.

Farifteh, J. 2007. Imaging spectroscopy of salt-affected soils: Model-based integrated method. PhD Diss. No. 143. ITC, Enschede, the Netherlands.

Fernandes, N.F., R.F. Guimarães, R.A.T. Gomes, B.C. Vieira, D.R. Montgomery, and H. Greenberg. 2004. Topographic controls of landslides in Rio de Janeiro: Field evidence and modeling. Catena 55:163–181.

Fernández Buces, N., C. Siebe, J.L. Palacio-Prieto, and R. Webster. 2009. Mapping soil salinity from sample data and remote sensing in the former Lake Texcoco, central Mexico. p. 291–304. *In* G. Metternicht and J.A. Zinck (ed.) Remote sensing of soil salinization: Impact on land management. CRC Press, Boca Raton, FL.

Giraut, M., P. Minotti, and S. Ludueña. 2000. Determinación de áreas de susceptibilidad hídrica a partir de imágenes Landsat TM y SAC-C sintético. *In* Proc. Simposio Latinoamericano de Percepción remota, 9th, Puerto Iguazú, Misiones, Argentina. 6–10 Nov. 2000. SELPER, Bogotá, Colombia.

Gómez, H., and T. Kavzoglu. 2005. Assessment of shallow landslide susceptibility using artificial neural networks in Jabonosa River Basin, Venezuela. Eng. Geol. 78:11–27.

Greesley, R., Ph. Christensen, and R. Carrasco. 1989. Shuttle radar images of wind streaks in the Altiplano, Bolivia. Geology 17:665–668.

Grings, F., M. Salvia, M. Barber, H. Karszenbaum, P. Ferrazzoli, F. Moccia, A. Soldano, D. Goniaski, G. Parmuchi, C. Montenegro, P. Kandus, and M. Borro. 2009. Monitoring soil condition in la Plata basin ecosystems using AMSR-E data. p. 1–9. *In* Aquarius/SAC-D Science Workshop, 4th, Puerto Madryn, Chubut, Argentina. 3–5 Dec. 2008. CONAE, Buenos Aires, Argentina.

Grings, F.M., P. Ferrazzoli, J.C. Jacobo-Berlles, H. Karszenbaum, J. Tiffenberg, P. Pratolongo, and P. Kandus. 2006. Monitoring flood condition in marshes using EM models and Envisat ASAR observations. IEEE Trans. Geosci. Rem. Sens. 44:936–942.

Guerra, A.J.T., J.K.S. Mendonça, M. Rêgo, and I.S. Alves. 2002. Gully erosion monitoring in São Luís City, Maranhão State, Brazil. *In* Proc. World Congress of Soil Science, 17th, Bangkok, Thailand. 14–21 Aug. 2002. IUSS, in CDRom.

Guinau, M., R. Pallas, and J.M. Vilaplana. 2005. A feasible methodology for landslide susceptibility assessment in developing countries: A case-study of NW Nicaragua after Hurricane Mitch. Eng. Geol. 80:316–327.

Hill, J., M. Stellmes, Th. Udelhoven, A. Roder, and S. Sommer. 2008. Mediterranean desertification and land degradation. Global Planet. Change 64:146–157.

Hoostsmans, R.M., A.F. Bouwman, R. Leemans, and G.J.J. Kreileman. 2001. Modelling land degradation in IMAGE 2. Rep. 481508009. National Institute of Public Health and the Environment, RIVM, the Netherlands.

Huete, A.R., X. Gao, H.H. Kim, T. Miura, C. Borghi, and R. Ojeda. 2002. Characterization of land degradation in central Argentina with hyperspectral AVIRIS and EO-1 data. *In* 17th World Congress of Soil Sci. CD-ROM Proc.: Confronting new realities in the 21st century, Bangkok, Thailand. 14–21 Aug. 2002. Paper no. 987. Kasetsart Univ., Bangkok.

Huete, A.R., T. Miura, and X. Gao. 2003. Land cover conversion and degradation analyses through coupled soil-plant biophysical parameters derived from hyperspectral EO-1 Hyperion. IEEE Trans. Geosci. Rem. Sens. 41:1268–1276.

Ishikawa, A.S., and E.A.D. Silva. 2007. Detecção de áreas inundadas utilizando imagens CBERS-2/CCD através de técnicas de morfología matemática. p. 1273–1280. *In* Anais Simpósio Brasileiro de Sensoramiento Remoto,

13th, Florianópolis, Brasil. INPE, São Paulo, Brasil.

Kandus, P., R.D. Quintana, and R.F. Bó. 2006. Landscape patterns and biodiversity of the lower delta of the Paraná river. Grupo de Investigaciones en Ecología de Humedales (GIEH), Departamento de Ecología, Genética y Evolución, Facultad de Ciencias Exactas y Naturales, Universidad nacional de Buenos Aires, Buenos Aires, Argentina.

King, C., N. Baghdadi, V. Lecomte, and O. Cerdan. 2005. The application of remote-sensing data to monitoring and modelling of soil erosion. Catena 62:79–93.

Koning, N., and E. Smaling. 2005. Environmental crisis or 'lie of the land'? The debate on soil degradation in Africa. Land use policy 22:3–11.

Koohafkan, P., D. Lantieri, and F. Nachtergaele. 2003. Land Degradation Assessment in Drylands (LADA): Guidelines for a methodological approach. Land and Water Development Div., FAO, Rome.

Lal, R., and B. Stewart. 1990. Soil degradation: A global threat. Springer-Verlag, New York.

Larsen, M.C., and A.J. Torres Sánchez. 1998. The frequency and distribution of recent landslides in three montane tropical regions of Puerto Rico. Geomorphology 24:309–331.

Liu, W.T.H., F.M. Ayres, E.L. Santiami, and P.J. Kanazawa. 2003. Pantanal inundation area prediction from space. p. 2523–2530. Anais Simpósio Brasileiro de Sensoramiento Remoto, 11th, Belo Horizonte, Brasil. INPE, São Paulo, Brasil.

Lobell, D., J. Ortiz-Monasterio, F. Cajigas-Gurrola, and L. Valenzuela. 2007. Identification of saline soils with multiyear remote sensing of crop yields. Soil Sci. Soc. Am. J. 71:777–783.

López, D., and J.M. Nuñez. 2006. Análisis de susceptibilidad a deslizamientos mediante el procesamiento de datos del programa de mapeo de radar topográfico SRTM. *In* Proc. Int. Symp. Sociedad Latinoamericana de Percepción Remota y Sistemas de Información Espacial, 12th, Cartagena, Colombia. 24–29 Sept. 2006. SELPER, Bogotá, Colombia.

López, H.J., and J.A. Zinck. 1991. GIS-assisted modelling of soil-induced mass movement hazards: A case study of the upper Coello river basin, Tolima, Colombia. ITC J. 4:202–220.

Madrigal, L.P., C.L. Wiegand, J.G. Merz, B.D. Rubio, X.C. Estrada, and O.L. Ramirez. 2003. Soil salinity and its effect on crop yield: A study using satellite imagery in three irrigation districts. Ingeniería Hidráulica en México 18:83–97.

Maldonado, F.D., G.S. de Salmuni, and E.D. Graffigna. 2001. Identificação e Caracterização da degradação na planicie aluvial do Semi-árido utilizando a combinação de imagens de interferometria ERS com imagens Ópticas Landsat TM. *In* Proc. Simposio Brasileiro de Sensoriamento Remoto, 10th, Foz do Iguazú, Brasil. INPE, São Paulo, Brasil.

Marcelino, E.V., L.M.G. Fonseca, F. Ventura, and A.N.C.S. Rosa. 2003. Evaluation of IHS, PCA and wavelet transform fusion techniques for the identification of landslide scars using satellite data. p. 487–494. *In* Anais Simpósio Brasileiro de Sensoriamento Remoto, 11th, Belo Horizonte, Brasil. 5–10 Apr. 2003. INPE, São Paulo, Brasil.

Martínez Gutiérrez, G. 2006. Aplicación de Sistemas de Información Geográfica e imágenes satelitales en la delineación de áreas propensas a inundaciones en Baja California Sur, México. p. 1–6. *In* C. Serafini (ed.) Proc. Int. Symp. Sociedad Latinoamericana de Percepción Remota y Sistemas de Información Espacial, 12th, Cartagena, Colombia. 24–29 Sept. 2006. SELPER, Bogotá, Colombia.

Mathieu, R., B. Cervelle, D. Rémy, and M. Pouget. 2007. Field-based and spectral indicators for soil erosion mapping in semi-arid mediterranean environments (Coastal Cordillera of central Chile). Earth Surf. Processes Landforms 32:13–31.

Mazzoni, E., and M. Vazquez. 2004. Ecosistemas de mallines y paisajes de la Patagonia Austral (provincia de Santa Cruz). INTA, Santa Cruz, Argentina.

Menéndez-Duarte, R., J. Marquínez, and G. Devoli. 2003. Slope instability in Nicaragua triggered by Hurricane Mitch: Distribution of shallow mass movements. Environ. Geol. 44:290–300.

Metternicht, G. 1998. Fuzzy classification of JERS-1 SAR data: An evaluation of its performance for Soil Salinity mapping. Int. J. Ecol. Modell. 111:61–74.

Metternicht, G. 2007. Remote sensing. p. 365–368 *In* K. Kemp (ed.) Encyclopedia of geographic information science. Sage Publ., New York.

Metternicht, G. 2003. Categorical fuzziness: A comparison between crisp and fuzzy class boundary modelling for mapping salt-affected soils using Landsat TM data and a classification based on anion ratios. Ecol. Modell. 168:371–389.

Metternicht, G., and J.A. Zinck. 2009. Spectral behavior of salt types. p. 21–37. *In* G. Metternicht and J.A. Zinck (ed.) Remote Sensing of Soil Salinization: Impact on Land Management. CRC Press, Boca Raton, FL.

Metternicht, G.I. 1996. Detecting and Monitoring Land Degradation Features and Processes in the Cochabamba Valleys, Bolivia: A Synergistic Approach. PhD Diss. No. 36. ITC, Enschede, the Netherlands.

Metternicht, G.I., and A. Fermont. 1998. Estimating Erosion Surface Features by Linear Mixture Modeling. Remote Sens. Environ. 64:254–265.

Metternicht, G.I., and J.A. Zinck. 1996. Modelling salinity-alkalinity classes for mapping salt-affected topsoils in the semiarid valleys of Cochabamba (Bolivia). ITC J. 2:125–135.

Metternicht, G.I., and J.A. Zinck. 1997. Spatial discrimination of salt- and sodium-affected soil surfaces. Int. J. Remote Sens. 18:2571–2586.

Metternicht, G.I., and J.A. Zinck. 1998. Evaluating de information content of JERS-1 SAR and Landsat TM data for discrimination of soil erosion features. ISPRS J. Photogramm. Remote Sens. 53:143–153.

Metternicht, G.I., and J.A. Zinck. 2003. Remote sensing of soil salinity: Potentials and constraints. Remote Sens. Environ. 85:1–20.

Mieza, M.S., F. Kovac, and R. Harán. 2004. Estimación de superficies inundadas mediante imágenes. SAC-C. *In* Proc. Simposio Latinoamericano de Percepción Remota, 11th, Santiago, Chile. 22–26 Nov. 2004. SELPER, Bogotá, Colombia.

Miranda, F.P.D., C.H. Beisl, and E.C.G. Camargo. 2007. Textural classification of R99SAR data as an aid to flood mapping in Coari City, Western Amazon Region, Brasil. p. 4935–4942. *In* Anais Simpósio Brasileiro de Sensoramiento Remoto, 13th, Florianópolis, Brasil. INPE, São Paulo, Brasil.

Moreiras, S.M. 2005. Landslide susceptibility zonation in the Rio Mendoza Valley, Argentina. Geomorphology 66:345–357.

Movia, C. 1980. Inventario de la erosión en la Patagonia Argentina basado en imágenes Landsat y fotografía aérea. p. 359–365. *In* Proc. Symposium Arid Land Resource Inventories: Cost-efficient methods, La Paz, México. 30 Nov.-6 Dec. 1980. Gen. Tech. Rep. WO-28, Washington, DC.

Naseri, M.Y. 1998. Characterization of salt-affected soils for modelling sustainable land management in semi-arid environment: A case study in the Gorgan region, Northeast Iran. PhD diss. Ghent University, Belgium.

Navone, S.M., C. Espoz-Alsina, A.E. Maggi, and R.M. Introcaso. 2002. Monitoreo de la desertificación en los valles semiáridos del noroeste argentino: Desarrollo de un Sistema de Información Geográfica empleando indicadores biofísicos y socioeconómicos. Revista de Teledetección 18:5–19.

Navone, S., E. Ezcurra, R. Introcaso, and I. Puentes. 2000. Sistema de información geográfica para el diagnostico de la erosión eólica en la laguna de pozuelos. *In* Proc. Simposio Latinoamericano de Percepción remota, 9th, Puerto Iguazú, Misiones, Argentina. 6–10 Nov. 2000. SELPER, Bogotá, Colombia.

Navone, S.M., and E. Palacín. 2004. Identificacion de la degradacion/desertificacion de las tierras en Santa Maria (Catamarca) a traves del procesamiento de imagenes Radarsat. Terra 18:289–297.

Ochoa-Tejeda, V., and J.F. Parrot. 2007. Extracción automática de trazas de deslizamientos utilizando un modelo digital de terreno e imágenes de satélite de alta resolución IKONOS. Ejemplo en la Sierra Norte de Puebla, México. Revista Mexicana de Ciencias Geológicas 24:354–367.

Okin, G.S., and D.A. Roberts. 2004. Remote Sensing in Arid Regions: Challenges and Opportunities. p. 111–146. *In* S. Ustin (ed.) Manual of remote sensing. John Wiley & Sons, New York.

Okoba, B.O., and G. Sterk. 2006. Quantification of visual soil erosion indicators in Gikuuri catchment in the central highlands of Kenya. Geoderma 134:34–47.

Palacio-Prieto, J.L., and J. López-Blanco. 1994. Videography: An alternative remote sensing tool for monitoring gully erosion. ITC J. 3:233–237.

Pallàs, R., J.M. Vilaplana, M. Guinau, E. Falgas, X. Alemany, and A. Munoz. 2004. A pragmatic approach to debris flow hazard mapping in areas affected by Hurricane Mitch: Example from NW Nicaragua. Eng. Geol. 72:57–72.

Paolini, L., J.A. Sobrino, and J.C. Jiménez-Muñoz. 2002. Detección de deslizamientos de ladera mediante imágenes Landsat TM: El impacto de estos disturbios sobre los bosques subtropicales del noroeste de Argentina. Revista de Teledetección 18:21–27.

Parmuchi, M.G., H. Karszenbaum, P. Kandus, and J. Tiffenberg. 2000. Clasificación de ambientes y alcance de inundación en el Bajo Delta del Río Paraná mediante imágenes multitemporales Radarsat-SAR. p. 1144–1153. *In* C. Serafini (ed.) Proc. Simposio Latinoamericano de Percepción remota, 9th, Puerto Iguazú, Misiones, Argentina. 6–10 Nov. 2000. SELPER, Bogotá, Colombia.

Paruelo, J.M., E. Jobbagy, and O. Sala. 2001. Current distribution of ecosystem functional types in temperate South America. Ecosystems 4:683–698.

Perotto-Baldiviezo, H.L., T.L. Thurow, C.T. Smith, R.F. Fisher, and X.B. Wu. 2004. GIS-based spatial analysis and modeling for landslide hazard assessment in steeplands, southern Honduras. Agric. Ecosyst. Environ. 103:165–176.

Ponce-Hernandez, R. 2002. Land degradation assessment in drylands. Approach and development of a methodological framework. Consultancy Report. AGLL, FAO. Rome.

Recatalá-Boix, L., and J.A. Zinck. 2008. Land-use planning in the Chaco Plain (Burruyacú, Argentina): Part 2: Generating a consensus plan to mitigate land-use conflicts and minimize land degradation. Environ. Manage. 42:200–209.

Riedel, P.S., A.R. Gomes, C.M. Bentz, M.F. Vidotti, and V. Liesemberg. 2007. Integração de técnicas de processamento digital de imagens e análise espacial na identificação de cicatrizes de escorregamento na região de Cubatão– Serra do Mar Paulista. p. 4393–4400. *In* Anais Simpósio Brasileiro de Sensoramiento Remoto, 13th, Florianópolis, Brasil. INPE, São Paulo, Brasil.

Roig, F.A., M.M. Gonzalez Loyarte, E.M. Abraham, E. Mendez, V.G. Roig, and E. Martinez Carretero. 1991. Maps of desertification hazards of Central Western Argentina, (Mendoza Province). Study case. *In* E. Arnold (ed.) World atlas of thematic indicators of desertification. UNEP, Londres.

Rosenqvist, A., B.R. Forsberg, T. Pimentel, Y.A. Rauste, and J.E. Richey. 2002. The use of spaceborne radar data to model inundation patterns and trace gas emissions in the central Amazon floodplain. Int. J. Remote Sens. 23:1303–1328.

Rostagno, C.M., F.R. Coronato, H.F. del Valle, and D.N. Puebla. 1999. Runoff and erosion in five land units of a closed basin of northeastern Patagonia. Arid Soil Res. Rehabil. 13:281–292.

Schernthanner, H. 2007. Application of the fuzzy logic method for landslide susceptibility mapping, as feasible-ready to use approach, in the context of development, Rio Blanco, Nicaragua. p. 114–122. *In* P. Zeil and S. Kienberger (ed.) Geoinformation for development: Bridging the divide through partnerships. Hüthig GmbH & Co. KG, Heidelberg, Germany.

Schomaker, M. 1997. Development of environmental indicators in UNEP. Land qQuality indicators and their use in sustainable agriculture and rural development. p. 35–56. *In* Proc. Workshop FAO, Rome. 25–26 Jan. 1996. FAO, Rome.

Sestini, M.F., and T.G. Florenzano. 2004. Caracterização de cicatrizes de deslizamentos por processamento de dados TM Landsat em Caraguatatuba-SP. Geologia USP Série Cientifica, São Paulo, Brasil. 4:57–69.

Sippel, S.J., S.K. Hamilton, J.M. Melack, and E.M.M. Novo. 1998. Passive microwave observations of inundation area and the area/stage relation in the Amazon River floodplain. Int. J. Remote Sens. 19:3055–3074.

Sonneveld, B.G.J.S. 2003. Formalizing expert judgments in land degradation assessment: A case study for Ethiopia. Land Degrad. Dev. 14:347–361.

Sonneveld, B.G.J.S., and D.L. Dent. 2009. How good is GLASOD? J. Environ. Manage. 90:274–283.

Sotomonte, S. 2007. Aplicación y ajuste del modelo de distribucion de carcavas de Vasquez-Selem y Zinck, caracterizando la susceptibilidad de erosion en el piedemonte de la zona sur, Sacaba (Cochabamba-Bolivia). MSc. diss. Centro de Levantamientos Aeroespaciales y aplicaciones SIG para el Desarrollo Sostenible de los Recursos Naturales (CLAS), Universidad Mayor de San Simón, Cochabamba, Bolivia.

Trueba Espinosa, A., J.L. Oropeza Mota, C.A. Ortiz Solorio, A. Martínez Alcántara, and G. Ruelas Ángeles. 2004. Identificación de zonas erosionadas mediante el tratamiento de imágenes digitales con una red neuronal. Agrociencia 38:573–581.

UNEP. 2004. GEO Latin America and the Caribbean Environment Outlook 2003. United Nations Environment Programme, Nairobi.

UNEP. 2007. GEO-4: Global environmental outlook. Environment for development. United Nations Environ. Programme, Nairobi.

Van Westen, C.J., E. Castellanos, and S.L. Kuriakose. 2008. Spatial data for landslide susceptibility, hazard, and vulnerability assessment: An overview. Eng. Geol. 102:112–131.

Vargas Cuervo, G. 1997. Evaluación de imágenes de satélite SAR ERS-1 y SPOT-Landsat en la cartografía de movimientos en masa. p. 109–118. *In* T.D. Guyenne (ed.) Proc. Int. Seminar Use and Applications of ERS in Latin America, Viñas del Mar, Chile. 25–29 Nov. 1997. ESA SP-405, Paris.

Vázquez-Selem, L., and J.A. Zinck. 1994. Modelling gully distribution on volcanic terrains in the Huasca area, central Mexico. ITC J. 3:238–251.

Veneziani, P., A.R. Santos, E. Crepani, C.E. Anjos, and R. Okida. 1998. Mapa de classes de erodibilidade de parte da região do Rio Taquari baseado em imagens TM-Landsat. Pesquisa Agropecuária Brasileira, Brasília, Brasil. 33:1747–1754.

Vente, J.D., J. Poesen, G. Verstraeten, A.V. Rompaey, and G. Govers. 2008. Spatially distributed modelling of soil erosion and sediment yield at regional scales in Spain. Global Planet. Change 60:393–415.

Vrieling, A., and S.C. Rodrigues. 2005. Erosion assessment in the Brazilian Cerrados using multi-temporal SAR imagery. *In* Proc. Envisat & ERS Symposium, Salzburg, Austria, 6–10 Sept. 2004. ESA SP-572, Paris.

Vrieling, A., S.C. Rodrigues, H. Bartholomeus, and G. Sterk. 2007. Automatic identification of erosion gullies with ASTER imagery in the Brazilian Cerrados. Int. J. Remote Sens. 28:2723–2738.

Wessels, K.J., S.D. Prince, and I. Reshef. 2007. Mapping land degradation by comparison of vegetation production to spatially derived estimates of potential production. J. Arid Environ. 72:1940–1949.

Winjnhoud, S., and N.H. Monteith. 1982. Suelos de la zona Ingeniero Jacobacci-Maquinchao. p. 129–156. *In* Instituto Nacional de Tecnología Agropecuaria (ed.) Sistemas Fisiográficos de la Zona Ingeniero Jacobacci-Maquinchao. FAO-INTA, Río Negro, Argentina.

WRI. 1995. World Resources 1994–1995: People and the environment, resource consumption, population growth and women. World Resources Institute, in collaboration with United Nations Environment Programme and United Nations Development Programme. Oxford Univ. Press, New York.

Zinck, J.A. (ed.). 2006. Land use change and land degradation in the western Chaco, Tucuman province, northwest Argentina. ITC Publ. 84. ITC, Enschede, the Netherlands.